New Technological Approach to Improve Gas Production from Class 2 Hydrate Deposits by Utilizing CO_2 Sequestration

Prathyusha Sridhara,[1,2] Brian J. Anderson,[1,2] Yongkoo Seol,[1] Evgeniy M. Myshakin[1,3]*

[1] *National Energy Technology Laboratory, 3610 Collins Ferry Road, P.O. Box 880, Morgantown, WV 26507, USA*
[2] *West Virginia University, Chemical Engineering, P.O. Box 6009, Morgantown, WV 26506, USA*
[3] *AECOM, 626 Cochran's Mill Road, P.O. Box 10940, Pittsburgh, PA 15236, USA*

* Corresponding author: evgeniy.myshakin@netl.doe.gov

Abstract

Numerical studies of the enhanced gas production from Class 2 hydrate accumulations using the CO_2-assisted technique was performed. The approach consists of three stages using a vertical well which serves as an injector during the first stage and as a producer in the third stage. First, CO_2 is injected into the aquifer, then the well is shut down to allow conversion of injected CO_2 into immobile hydrate phase. After CO_2 hydrate is formed, decomposition of CH_4 hydrate is induced by the depressurization method to estimate production over 15 years. The results show that methane production is increased accompanied with simultaneous reduction of concomitant water production comparing to conventional Class 2 reservoir performance.

Introduction

There are several methods for recovering natural gas from hydrate accumulations.[1,2] The most practical methods include depressurization, thermal stimulation, chemical inhibitor injection methods, and CO_2-CH_4 exchange in CH_4-hydrates.[4] Besides CH_4 production the last technique provides simultaneous sequestration of the greenhouse gas in a form of hydrate. The feasibility of the swapping process is owed to the following reasons, 1) CO_2, CH_4 and mixtures of these gases form the same crystallographic structure, Type I hydrate.[6,7] This structural similarity assists in maintaining the structural integrity after swapping of CH_4 by CO_2 in the natural gas hydrate settings and no stiffness loss is observed at the sediment scale.[8] 2) CO_2-hydrate is thermodynamically more stable than CH_4-hydrate at temperatures and pressures typical for geological methane hydrate accumulations.[9] The disadvantage of the method is related to low permeability of a hydrate-bearing formation making the migration of injected and released gases a slow process. This work utilizes CO_2 injection into highly-permeable aquifer beneath methane hydrate-bearing sand (Class 2 hydrate accumulations[10,11]) to form CO_2 hydrate. The natural gas production enhancement is achieved by using the heat released during CO_2 hydrate formation to support the methane hydrate decomposition reaction and by reduction of water production from the aquifer.

Numerical details

Reservoir simulator - Mix3HydrateResSim

There are several popular reservoir simulators available to study gas hydrates: CMG STARS[13], HydrateResSim[14], MH-21 HYDRES[15], STOMP-HYD[16], TOUGH+HYDRATE.[17] HydrateResSim (HRS) is the open-source code available for the public at the National Energy Technology Laboratory (NETL). It accounts for five components (CH_4, H_2O, hydrate, inhibitors and a heat pseudo-component) distributed among four phases (gas, liquid, ice and hydrate) to model the non-isothermal gas release, phase behavior, and flow of fluids and heat in complex geological media. HRS includes equilibrium models of non-isothermal formation and dissociation of single CH_4-hydrate. Recently, the equilibrium model was modified to account for formation and dissociation of ternary hydrates (CH_4-CO_2-N_2 hydrate) and produce a new version, Mix3HydrateResSim (Mix3HRS)[3]. Mix3HRS allows distribution of six components (CH_4, CO_2, N_2, H_2O, water-soluble inhibitors and a heat pseudo-component) among four possible phases (gas, liquid, ice, and hydrate). Along with the phase equilibrium data, new primary variables

are added for each phase state together with extra governing equations for CO_2 and N_2 components. The mixed hydrate equilibrium data obtained using the cell potential[18] are incorporated in to code in a tabular form and a tri-linear interpolation is used to interpolate data at given pressure and temperature conditions:

$$T_{eq} = f(P, yCO_2, yCH_4) \quad \& \quad P_{eq} = g(T, yCO_2, yCH_4)$$

where, T is temperature (^{0}C), P is pressure (Pa), yCO_2 is CO_2 composition in gas phase and yCH_4 is CH_4 composition in gas phase. The mass and energy balance equations are discretized in space using the integral finite difference method and by forward first-order finite difference and a fully implicit approach in time. This time discretization results in a set of coupled non-linear algebraic equations obtained for each volume element. These equations completely define the state of the flow system at a time level and are solved by Newton/Raphson iteration. In this work, numerical simulations were performed using Mix3HRS code.

Geometry and stratigraphic units

The reservoir model considered in this work is axisymmetric representing a cylindrical domain suitable to study radial flow near the vertical well.[19] Taking an advantage of the symmetry, the reservoir is represented as a 2D model as a vertical cross-section along its radius (Figure 1). In the lateral direction, the grid extends out to 500 m, which is discretized into 75 grid blocks, with logarithmically distributed lengths, to ensure fine discretization around the wellbore. The total thickness of the reservoir domain is 40 m. It consists of the sand formation (20 m) bounded at the top and bottom by shale layers (10 m each). The sand formation is split into the hydrate-bearing sand (13 m, Zone 1 in Figure 1) and the water-bearing sand (8 m, Zone 2 in Figure 1) representing a typical Class 2 hydrate accumulation.[2] In the vertical direction the over- and under-burden are discretized into sub-layers of 2 m thickness and the hydrate-bearing and water-bearing sands have sub-layers of 1 m thickness. The top and bottom boundaries of the reservoir are set at fixed temperature conditions providing heat influx into the formation with no mass flow allowed. The lateral boundaries are taken as impermeable for both heat and mass transfer. A vertical wellbore of radius 0.11 m is completed through the sand formation (Figure 1).

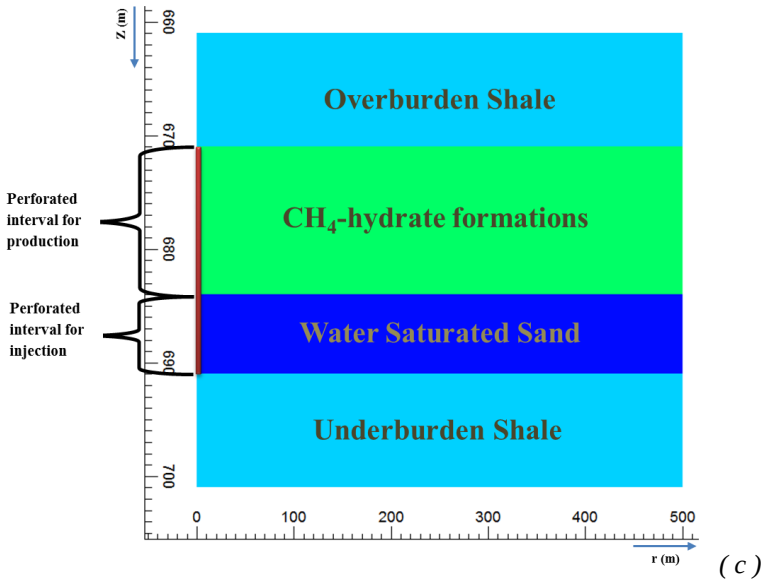

Figure 1: The 2D radial model used for simulations. The green layer is Zone 1 (methane-hydrate bearing sand) and the deep blue layer is Zone 2 (water-bearing sand).

Reservoir properties

The CH_4 hydrate layer (Zone 1) extends from 673 m to 685 m with the hydrate-water contact set at a depth of 685 m (2248 ft), the typical depth of Prudhoe Bay L-Pad region of Alaska North Slope[10]. The geological deposit are assumed to be high-quality sand formation with uniform hydrate saturations, S_h = 70%. Uniform values for porosity, saturations, intrinsic permeability, and irreducible water saturation are assumed in the simulations (Table 1).

Relative permeability and capillary pressure values are calculated using Brooks and Corey[21] and Van Genuchten[22] functions, respectively (Table 2).

Table 1: Reservoir parameters used in the simulations.

Parameters	Value
Rock Grain Density (kg/m^3)	Zones 1 and 2 - 2600
	Shale- 2600
Porosity (%)	Zones 1 and 2- 35
	Shale- 10
Intrinsic Permeability (mD)	Zone 1 - 0
	Zone 2 - 1000
	Shale- 0
Rock grain specific heat (J/kg ˚C)	Zones 1 and 2 - 1000
	Shale - 1000
Thermal conductivity (W/m K)	Zone 1 and 2 - 3.0
	Shale - 3.1
Pore Compressibility (Pa^{-1})	5.0×10^{-10}

Table 2: Parameters used for relative permeability and capillary pressure functions.

Relative Permeability	Brooks and Corey $k_{rA} = (S_A^*)^n;\ k_{rG} = (S_G^*)^n$ $S_A^* = \frac{(S_A - S_{irA})}{(1 - S_{irA})};\ S_G^* = \frac{(S_G - S_{irG})}{(1 - S_{irG})}$
Irreducible water saturation, S_{irA}	0.10
Irreducible gas saturation, S_{irG}[23]	0.001
n[23]	3
Capillary pressure	Van Genuchten Function $P_{cap} = -P\left[(S^*)^{-1/\lambda} - 1\right]^{\lambda}\ S^* = \frac{(S_A - S_{irA})}{(S_{\max A} - S_{irA})}$
Irreducible water saturation, S_{irA}	0.09
λ[3]	0.45
S_{maxA}	1
P_{max}, *Pa*[3]	1.25×10^4

Initial conditions

Initial pore pressure of the system is assumed to follow hydrostatic pressure distribution.[24] Temperature of the reservoir is assigned based on the local geothermal gradient (0.033 ℃/m[20]). Figure 2 displays the initial distributions of pressure and temperature in the reservoir. The CH_4 hydrate sand formation (Zone 1, Figure 1) is modeled as a two-phase system with aqueous phase (30%) in equilibrium with hydrate phase (70%) in pore space. The water-bearing sand formation (Zone 2, Figure 1) and over- and underburden shales are considered to have pores filled with aqueous phase only.

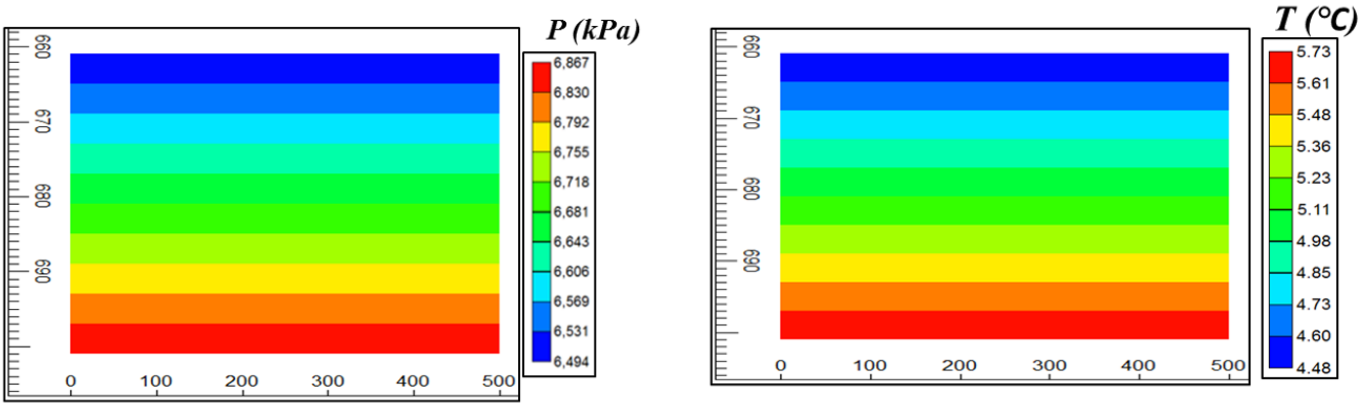

a) **b)**

Figure 2: Initial pressure (a) and temperature (b) distributions in the reservoir model

Technological approach

The approach encompasses three stages and is conducted in a 'huff and puff' style, where a single vertical wellbore is used as an injector in the first stage and later as a producer in the third stage. During the Stage I, the wellbore is completed throughout the Zone 2 (Figure 1) to inject pure CO_2 into the water-bearing sand formation. Injection is continued till the onset of CO_2 hydrate formation is observed at the advancing front of the injected fluid in Zone 2. At the next Stage II, the wellbore is shut-off and the reservoir is left "idle" allowing pressure and temperature conditions in Zone 2 reach the CO_2 hydrate stability region on the phase diagram to induce and maintain the hydrate formation reaction. Consequently, at Stage III, the dissociation of CH_4 hydrates is initiated by the depressurization method using the well interval completed throughout the Zone 1 (Figure 1). The methane production benefits from heat accumulated in Zone 2, *i.e.*, contributions from the exothermic nature of gas dissolution in water and CO_2 hydrate formation reaction. Additionally the gas productivity is increased by means of reduced permeability of Zone 2 that limits water influx into the producing well bore. Hence, along with depressurization, this method employs *in situ* thermal stimulation, which promotes release of gas from CH_4 hydrate. Stages I-III are described in details in the next sections.

Injection stage (Stage I)

Pure CO_2 is injected at a constant flow rate of 162 metric ton/day (82 x 10^3 ST m^3/day) and specific enthalpy of –252.5 kJ/kg (at T = 13°C). In 2012, during the Ignik-Sikumi field test, ConocoPhilips conducted the step rate test to measure the Formation Parting Pressure (FPP) of *in situ* hydrate sediments located in the Prudhoe Bay Unit on the Alaska North Slope. The FPP value was estimated to be 9.86 MPa[10]. In our simulations to maintain the wellbore integrity, the injection flow rate is selected such that the pressure build up around the wellbore remains lower than the fracture initiation pressure (9.86 MPa). The temperature of injected CO_2 must be greater than 10.5°C[25] to ensure that no CO_2 hydrate forms around the wellbore that would lower gas permeability in the reservoir and plug CO_2 plume propagation in the aquifer. The injection of CO_2 continues till the onset of hydrate formation takes place in the reservoir after 145 days. During that time, 23,490 metric ton of CO_2 is injected.

Figure 3 displays the pressure, temperature, CO_2 and water saturation distributions at the end of injection. The CO_2 plume displaces water and increases the gas saturation in the domain up to 0.8 (Figure 3c) in the vicinity of the wellbore. Figure 3b shows the temperature increase in the reservoir following to the CO_2 saturation advance. The temperature is risen due to two processes accounted in the code: (1) the specific enthalpy of injected CO_2; (2) the exothermic nature of CO_2 dissolution in water (CO_2 (gas) $\rightarrow$ CO_2 (aq); Q = -19.4 kJ/mol[26] for pure water at 15 ^oC). Because of the heat exchange with the surrounding formations, the temperature declines as the CO_2 plume propagates in the reservoir (Figure 3b).

The onset of CO_2 hydrate formation is predicted after 145 days at a radial distance of 85 m. By this time, the pressure buildup around the wellbore reaches 9 MPa (Figure 3a), hence any further injection would exceed the

fracture initiation pressure. Moreover, hydrate formation hinders further fluid flow as it lowers the effective permeability of the aquifer. The wellbore is shut off and the reservoir domain is set to equilibrate with the surroundings to bring pressure and temperature conditions into the CO_2 hydrate stability region.

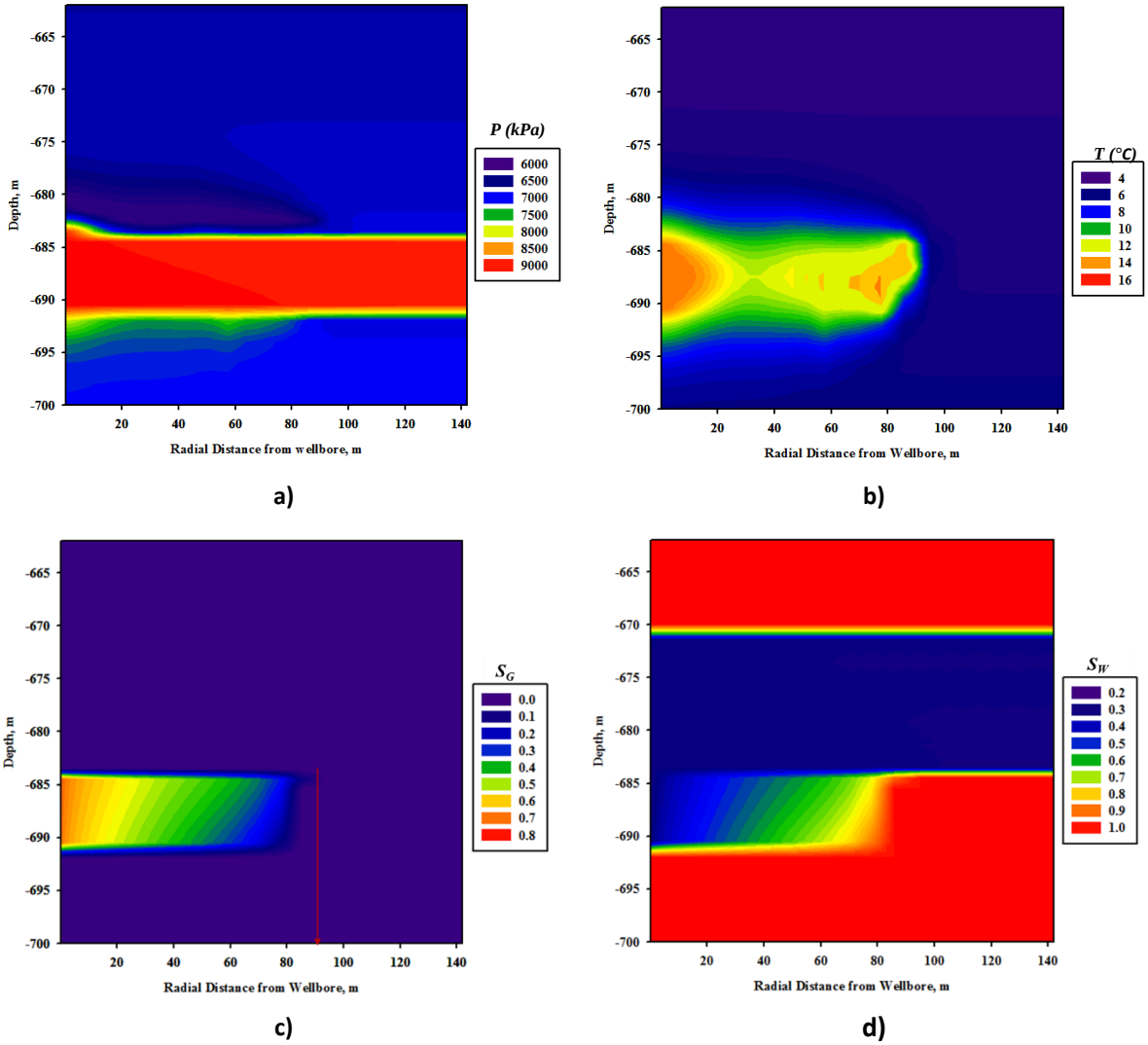

Figure 3. Contour plots showing pressure distribution (a), temperature distribution (b), CO_2 gas saturation (c), and water saturation (d) after 145 days of injection. The red arrow indicates the distance at which hydrate formation evolves.

Equilibration stage (Stage II)

To enable CO_2 hydrate formation in Zone 2, the temperature should drop below 10-10.5 ^oC at the pressure around 8 MPa according the equilibrium phase diagram. Figure 4 shows the conditions of the reservoir at the end of 2.5 years of equilibration. CO_2 hydrate saturation starts forming at the top and bottom boundaries of the CO_2 plume in Zone 2 (Figure 4d) because these regions are closer to the heat sinks (Zone 1 and underburden shale) that support temperature gradients. The temperature distribution shows that the temperature is decreased (comparing to Figure 3b) to hydrate equilibrium temperature, thus promoting hydrate formation (Figure 4b). The CO_2 hydrate formation causes water flow from Zone 1 that results in local pressure decrease in Zone 1 inducing partial methane hydrate decomposition and formation of mixed hydrates at the boundary between Zones 1 and 2. The gas saturation distribution indicates that its values decreased owing to CO_2 conversion into hydrate phase (Figures 3c and 4c).

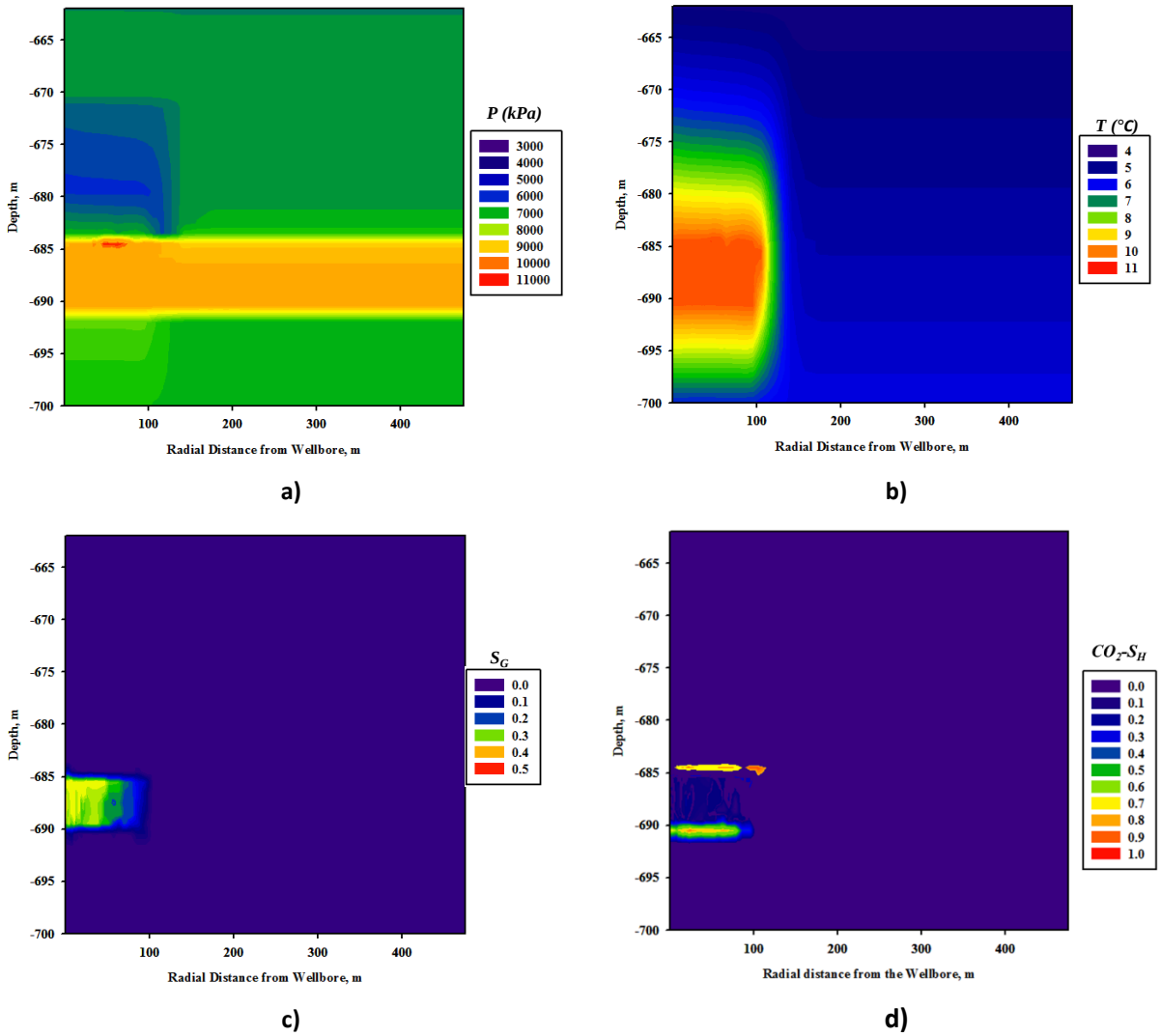

Figure 4: Contour plots showing pressure distribution (a), temperature distribution (b), CO_2 gas saturation (c), and CO_2 hydrate saturation (d) distributions after 2.5 years since the beginning of Stage II.

Duration of Stage II controls the heat released from the CO_2 hydrate formation and the exothermic CO_2/CH_4 exchange reactions (enthalpy of CO_2 hydrate formation is from -57.7 to -63.6 kJ/mol[27] while enthalpy of methane hydrate decomposition is from 52.7 to 55.4 kJ/mol[28]) and extent of CO_2 hydrate formation in Zone 2. Hence, duration of Stage II provides a significant impact on methane production volumes in the subsequent Stage III. To study the effect, three cases were considered using 2.5, 3.5 and 8 years as Stage II's time periods. Cases 1-3 are characterized with different initial local CO_2 hydrate saturation level in the top layer of Zone 2 within first 100 m from the well bore (the second number in the first column of Table 3). Table 3 collects the time periods for all stages carried out in the study. Besides different CO_2 saturations, the cases vary in their initial conditions of the reservoir before the commencement of Stage III due to varied durations of Stage II. The base Case 4 is considered to compare results with those at Cases 1-3. It mimics production from a conventional Class 2 gas hydrate accumulation at which the first two stages are not performed.

Table 3: The duration of stages for the Cases considered.

Case number / CO_2 hydrate saturation	**Stage I**	**Stage II**	**Stage III**
	Time, years		

Case 1 / 0.7	0.45	2.5	15.0
Case 2 / 0.8	0.45	3.5	15.0
Case 3 / 0.9	0.45	8.0	15.0
Case 4 / 0.0	-	-	15.0

Production stage (Stage III)

The decomposition of methane hydrate in Zone 1 is induced by depressurizing the zone at a constant bottom-hole pressure (BHP) set at 3.5 MPa. That pressure value was chosen to maintain thermodynamic conditions within the CH_4 hydrate instability and CO_2 hydrate stability region on the phase diagrams. This ensures that the formed CO_2 hydrate in the aquifer remains intact during the Stage III as CH_4 hydrate in Zone 1 decomposes and release CH_4 and water.

Figure 5 displays the cumulative volumes of produced methane and corresponding production gas rates for all the cases for the 15 years. Cases 1-3 demonstrate production rates around 4,000 ST m^3/day after about 1 years of depressurization, and further Case 1 provides 5,800 ST m^3/day after 2 years of production. In contrast, Case 4 consistently displays low production rate, ~500 m^3/day over first 6 years. As a result, cumulative gas volumes produced after 15 years of depressurization are larger for Cases 1-3 comparing to Case 4 due to additional heat flux brought into the Zone 1 during Stages I-III and lowering the aquifer's permeability.

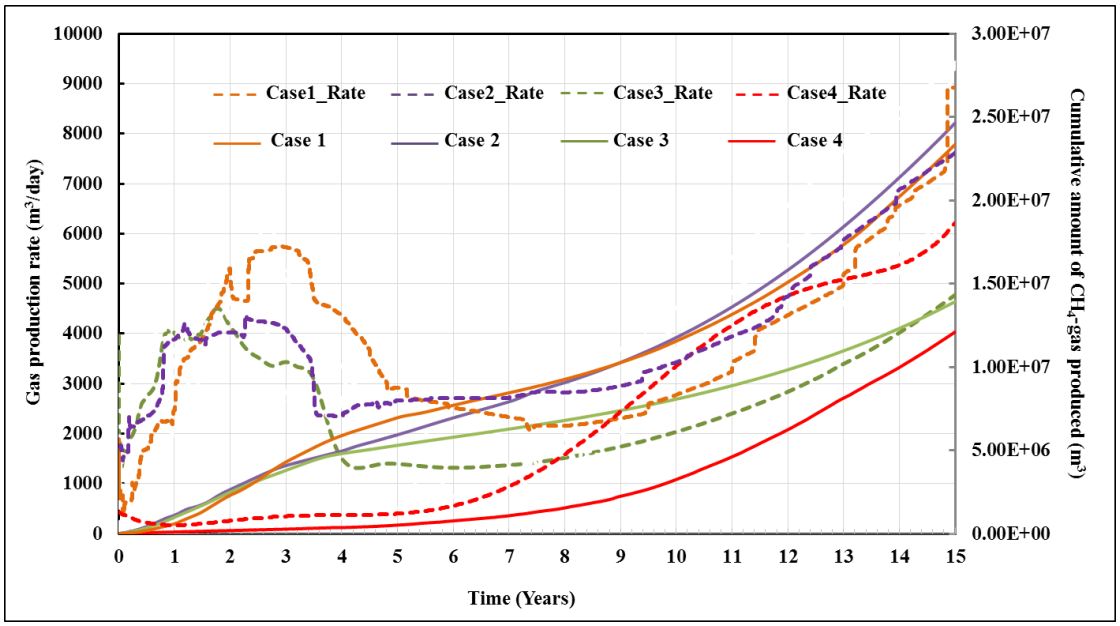

Figure 5: Gas production rates (dashed lines) and cumulative volume (solid lines) of gas produced for Cases 1-4. Time zero designates the onset of Stage III.

Figure 5 shows that production rates are the highest for Cases 2 and 3 in the beginning of depressurization. After 1.5 years the rate at Case 1 becomes higher that results in larger cumulative gas volumes produced up to approximately 9 years. At the end of Stage III gas volumes at Cases 1 and 2 become comparable, while production at Case 3 characterized with the longest Stage II falls in between Cases 1-2 and the base Case 4. It appears that the prolonged Stage II diminishes the effect of additional heat flux into the methane hydrate-bearing sands from Zone 2. That is a consequence of complex interplay of the contributing factors to the total heat flux across the Zone 1 – Zone 2 boundary attributed to conductive and advective heat transfer mechanisms as displayed in Equation 1:

$$F^h = \sum_\beta h_\beta F_\beta \; - \; K\,(\nabla T) \qquad (1)$$

where

h_β - specific enthalpy of phase β; F_β - mass flux of phase β; K - heat conductivity, T - temperature

As Stage III proceeds on, the increase in CO_2 hydrate saturation declines the effective permeability of the aquifer, which impedes the mass flow across the boundary. This lowers the contribution of the advective heat flow and makes the conductive heat transfer mechanism to be the major contributor to the total heat flux during depressurization. The combination of two mechanisms for heat transfer and continuous CO_2 hydrate formation supporting sensible heat in Zone 2 are the reasons of high production performance at Cases 1 and 2. Stage II is also needed to create a hydrate barrier along the Zone 1 - Zone 2 boundary to prevent CO_2 escape into Zone 1. The estimates of CO_2 breakthrough at the producing well bore are given below for the cases of interest.

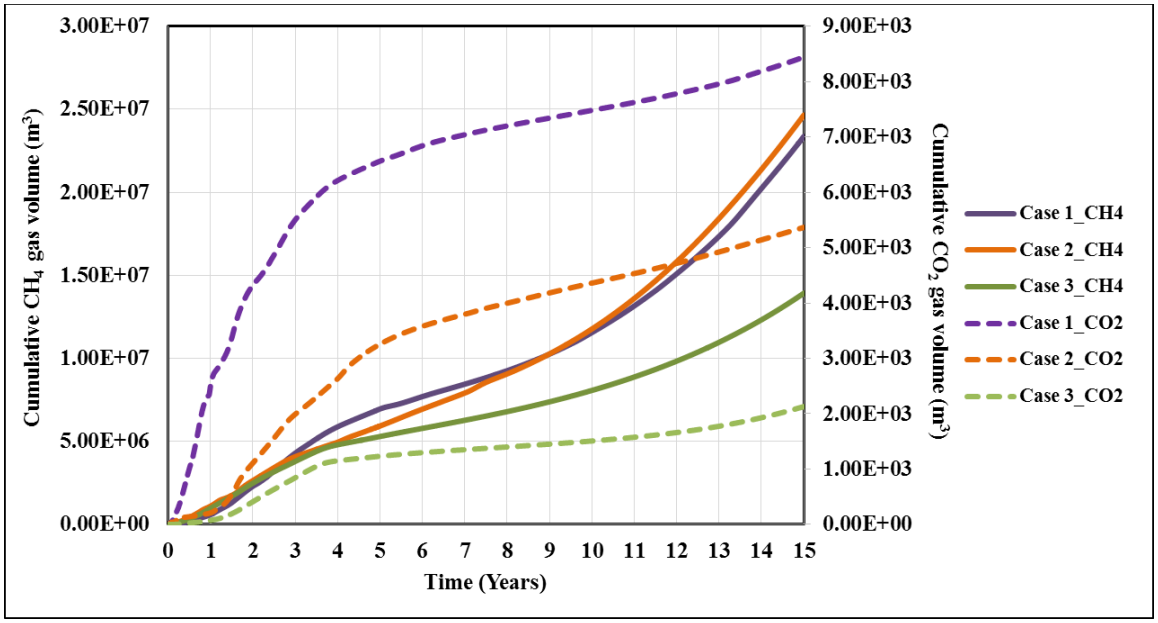

Figure 6: Cumulative volumes of CH_4 (Solid line) and CO_2 (dashed line) for Cases 1-3 in the production stream.

Figure 6 shows the cumulative amounts of CO_2 and CH_4 produced during the Stage III. Case 3 characterized by the highest initial CO_2 hydrate saturation in the aquifer at the boundary (Table 3) records the lowest volume of CO_2 in the production stream. In relative numbers the contribution of CO_2 in the total production gas volume is negligible, for Cases 1-3 it is estimated to be 0.02-0.04% at the end of 15 years. In respect of the total injected CO_2 (1.189×10^7 ST m^3) the amounts of CO_2 leakage into the producing stream are 0.07% (Case 1), 0.05% (Case 2), 0.02% (Case 3) on volume basis.

Cumulative volumes of water produced throughout the production period and the corresponding water production rates are depicted in Figure 7. The gas produced at Case 2 is twice higher than at Case 4 after 15 years (Figure 5), but the produced water volume for Case 2 is nearly same as Case 4. At the base Case 4 the most intensive water production occurs in the first year that is evidenced by the sharp increase of the water production rate (Figure 7). The larger water rate comparing to Cases 1-3 is directly attributed to the unhampered hydraulic communication between the producing well bore and the aquifer as soon as methane hydrate started to decompose at the Zone 1-Zone 2 boundary.

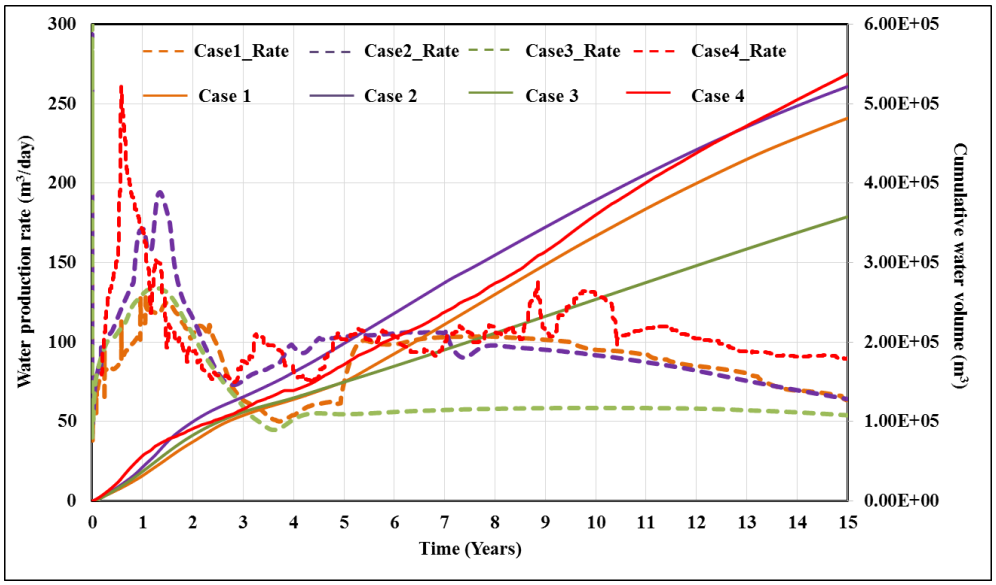

Figure 7: Water production rates (dashed lines) and cumulative volume (solid lines) of water produced for Cases 1-4. Time zero designates the onset of Stage III.

Conclusion

The technique reported in this study encompasses the benefits of *in situ* thermal stimulation in conjunction with depressurization to enhance methane production from geologic Class 2 hydrate deposits. The study proposes a novel technical approach, which utilizes heat transfer mechanisms into producing hydrate-bearing sediment from the underlying aquifer. The results show that the issue of vast production of water during the exploitation of Class 2 hydrate accumulations can be handled efficiently by means of CO_2 hydrate formation in the underlying aquifer. Simultaneously, CO_2 is effectively captured in hydrate lattice providing an attractive way for permanent carbon storage. Such technique does not require the presence of cap rock sealing a formation with injected mobile CO_2 to prevent unwanted CO_2 escape into the atmosphere.

Acknowledgment

This technical effort was performed in support of the National Energy Technology Laboratory's ongoing research under the RES contract DE-FE0004000.

Disclaimer

References

1. Moridis, G.J., Reagan, M.T., "Strategies for Gas Production from Oceanic Class 2 Hydrate Accumulations" *Offshore Technology Conference*, OTC-18866, 2007.

2. Moridis, G.J., Collett, T., Boswell, R., Kurihara, M., Reagan, M.T., Koh, C., Sloan, E.D., "Toward production from gas hydrates: current status, assessment of resources, and simulation-based evaluation of technology and potential", *SPE Reservoir Eval. Eng*. 12, 745-771, 2009.

3. Reservoir Simulation for Production of CH_4 from Gas Hydrate Reservoirs Using CO_2/CO_2+ N_2 by HydrateResSim ". Ph. D. thesis, West Virginia University, 2013

4. Ohgaki, K., et al., "Methane exploitation by carbon dioxide from gas hydrates. Phase equilibria for CO2-CH4 mixed hydrate system", *Journal of Chemical Engineering of Japan*, 29, 478-483, 1996.

5. Ors, O., Sinayuc, C. "An experimental study on the CO 2–CH 4 swap process between gaseous CO 2 and CH 4 hydrate in porous medi", *Journal of Petroleum Science and Engineering*, 119, 156-162, 2014.

6. Sloan Jr, E.D., Koh, C., "Clathrate hydrates of natural gases",CRC press, 2007.

7. Adisasmito, S., R.J. Frank III, Sloan, E. D. Jr, "Hydrates of carbon dioxide and methane mixtures", Journal of Chemical and Engineering Data, 1991. **36**(1): p. 68-71.

8. Jung, J., Santamarina, J.C. "CH_4-CO_2 replacement in hydrate-bearing sediments: A pore-scale study", *Geochemistry, Geophysics, Geosystems*, 11(12), 2010.

9. Kang, S.-P., Chun, M.-K., Lee, H., "Phase equilibria of methane and carbon dioxide hydrates in the aqueous $MgCl_2$ solutions", *Fluid Phase Equilibria*, 147, 229-238, 1998.

10. Anderson, B., et al. "Review of the Findings of the Iġnik Sikumi CO2-CH4 gas Hydrate Exchange Field Trial", *Proceeding, 8th International Conference on Gas Hydrates*, 2014.

11. Moridis, G. "Numerical simulation studies of thermally-induced gas production from hydrate accumulations with no free gas zones at the Mallik site, Mackenzie Delta, Canada", *SPE Asia Pacific Oil and Gas Conference and Exhibition*, 2002.

12. Ajayi, T., "Advanced Reservoir Modeling and Fluid Flow Studies of Natural Gas Production from the Hydrate Reservoirs of the Alaska North Slope", Ph.D. thesis, West Virginia University, 2016.

13. "Advanced Processes & Thermal Reservoir Simulator (STARS) User's Guide", Computer Modelling Group Ltd.

14. Moridis, G., Kowalsky, M., Pruess, K., "HydrateResSim Users Manual: A Numerical Simulator for Modeling the Behavior of Hydrates in Geologic Media", Lawrence Berkeley National Laboratory, 2005.

15. Kurihara, M., et al., "Assessment of gas productivity of natural methane hydrates using MH21 Reservoir Simulator. Natural Gas Hydrates: Energy Resource Potential and Associated Geologic Hazards" *Proceeding, AAPG Hedberg Conference*, 2004.

16. M.D.White, "STOMP subsurface transport over multiple phases, version 4.0, user's guide", PNNL-15782. Pacific Northwest National Laboratory, 2006.

17. Moridis, G., Kowalsky, M., Pruess, K., "ToughþHydrate v1. 0 User's Manual: A Code for the Simulation of System Behavior in Hydrate-Bearing Geologic Media", Lawrence Berkeley National Laboratory, 2008.

18. Anderson, B.J., et al., "Application of the cell potential method to predict phase equilibria of multicomponent gas hydrate systems", *Journal of Physical Chemistry B*, 109, 8153-8163, 2005.

19. Join, S., "Gridding in reservoir simulation".

20. Anderson, B.J., et al., "Regional long-term production modeling from a single well test, Mount Elbert gas hydrate stratigraphic test well, Alaska North slope", *J. Marine and petroleum geology*, 28, 493-501, 2011.

21. Brooks, R.H., Corey, A. T., "Hydraulic properties of porous media and their relation to drainage design", *Transactions of the ASAE*, 7, 26-0028, 1964.

22. Van Genuchten, M.T., "A closed-form equation for predicting the hydraulic conductivity of unsaturated soils." *Soil science society of America journal*, 44, 892-898, 1980.

23. Mahabadi, N., et al. "Water Retention Curve and Relative Permeability for Gas Production from Hydrate-Bearing Sediments" *AGU Fall Meeting Abstracts*. 2014.

24. Wright, J., Dallimore, S., Nixon, F., "Influences of grain size and salinity on pressure-temperature thresholds for methane hydrate stability in JAPEX/JNOC/GSC Mallik 2L-38 gas hydrate research-well sediments", Bulletin of Geological Survey of Canda, 229-240, 1999.

25. Bozzo, A.T., et al., "The properties of the hydrates of chlorine and carbon dioxide", *Desalination*, 16, 303-320, 1975.

26. Carroll, J.J., Slupsky, J.D., Mather, A.E., "The solubility of carbon dioxide in water at low pressure", *Journal of Physical and Chemical Reference Data*, 20, 1201-1209, 1991.

27. Anderson, G.K., "Enthalpy of dissociation and hydration number of carbon dioxide hydrate from the Clapeyron equation", *The Journal of Chemical Thermodynamics*, 35, 1171-1183, 2003.

28. Anderson, G.K., "Enthalpy of dissociation and hydration number of methane hydrate from the Clapeyron equation", *The Journal of Chemical Thermodynamics,* 36, 1119-1127, 2004.